Abstracta

Ano XIII - N. 03

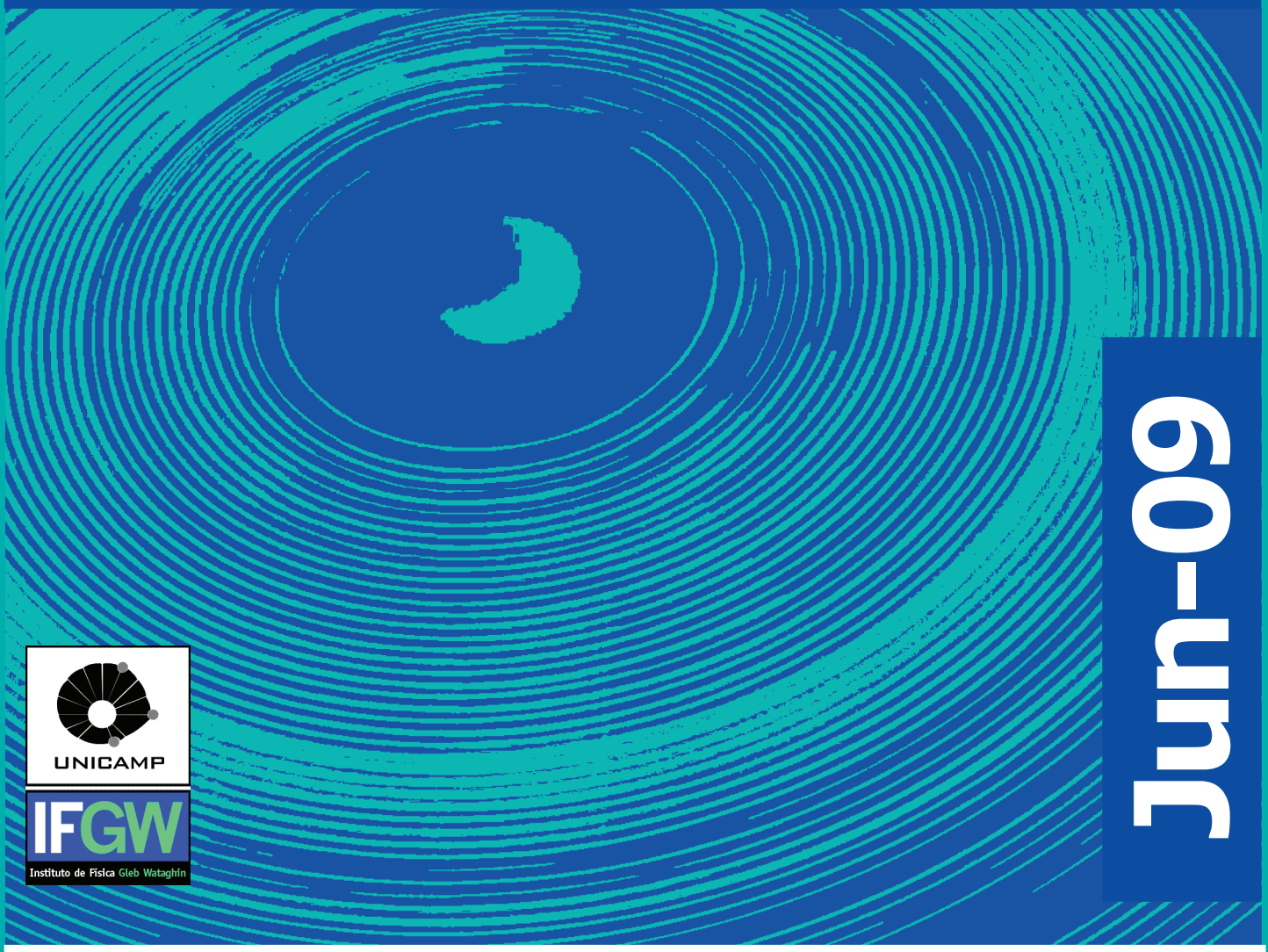

Jun-09

UNICAMP

IFGW

Instituto de Física Gleb Wataghin

Trabalhos Publicados

Maio 2009 à Junho 2009

P095-09 à P123 -09

Trabalhos Publicados

P095-09 "A General Approach to First Order Phase Transitions and the Anomalous Behavior of Coexisting Phases in the Magnetic Case"

Gama, S., de Campos, A., Coelho, A. A., Alves, C. S., Ren, Y., Garcia, F., Brown, D. E., da Silva, L. M., Carvalho, A. M. G., Gandra, F. C. G., dos Santos, A. O., Cardoso, L. P., and von Ranke, P. J.

First order phase transitions for materials with exotic properties are usually believed to happen at fixed values of the intensive parameters (such as pressure, temperature, etc.) characterizing their properties. It is also considered that the extensive properties of the phases (such as entropy, volume, etc.) have discontinuities at the transition point, but that for each phase the intensive parameters remain constant during the transition. These features are a hallmark for systems described by two thermodynamic degrees of freedom. In this work it is shown that first order phase transitions must be understood in the broader framework of thermodynamic systems described by three or more degrees of freedom. This means that the transitions occur along intervals of the intensive parameters, that the properties of the phases coexisting during the transition may show peculiar behaviors characteristic of each system, and that a generalized Clausius-Clapeyron equation must be obeyed. These features for the magnetic case are confirmed, and it is shown that experimental calorimetric data agree well with the magnetic Clausius-Clapeyron equation for MnAs. An estimate for the point in the temperature-field plane where the first order magnetic transition turns to a second order one is obtained (the critical parameters) for MnAs and Gd5Ge2Si2 compounds. Anomalous behavior of the volumes of the coexisting phases during the magnetic first order transition is measured, and it is shown that the anomalies for the individual phases are hidden in the behavior of the global properties as the volume

Advanced Functional Materials 19[6], 942-949. 2009.

P096-09 "A new ultra-high-vacuum variable temperature and high-magnetic-field X-ray magnetic circular dichroism facility at LNLS"

Figueiredo, J. J. S., Basilio, R., Landers, R., Garcia, F., and de Siervo, A.

X-ray magnetic circular dichroism (XMCD) is one of the most powerful tools for investigating the magnetic properties of different types of materials that display ferromagnetic behavior. Compared with other magnetic-sensitive techniques, XMCD has the advantage of being element specific and is capable of separating the spin and magnetic moment contributions associated with each element in the sample. In samples involving, for example, buried atoms, clusters on surfaces or at interfaces, ultrathin films, nanoparticles and nanostructures, three experimental conditions must be present to perform state-of-the-art XMCD measurements: high magnetic fields, low temperatures and an ultra-high-vacuum environment. This paper describes a new apparatus that can be easily installed at different X-ray and UV beamlines at the Brazilian Synchrotron Light Laboratory (LNLS). The apparatus combines the three characteristics described above and different methods to measure the absorption signal. It also permits in situ sample preparation and transfer to another chamber for measurement by conventional surface science techniques such as low-energy electron diffraction (LEED), reflection high-energy electron diffraction (RHEED), X-ray photoelectron spectroscopy (XPS) and X-ray photoelectron diffraction (XPD). Examples are given of XMCD measurements performed with this set-up on different materials

Journal of Synchrotron Radiation 16, 346-351. 2009.

P097-09 "An experiment on the effect of oxygen content and air velocity on soot formation in acetylene laminar diffusion flame produced in a burner with a parallel annular coaxial oxidizer flow"

Santos, A. A. B., Goldstein, L., and Ferrari, C. A.

The effect of oxygen content and of the combustion air velocity on soot formation was studied in acetylene diffusion flames. These flames were produced in a burner with a parallel annular coaxial flow of oxidizer. The effect on the flame axial temperature profile was also evaluated. The soot volume fraction was calculated by the laser light extinction methodology. The oxygen content in the combustion air was smaller than 30%, which does not require significant retrofit of existent equipment when the combustion conditions are varied. The results suggest that the parallel manipulation of the oxygen content and of the oxidizer velocity can provide means for managing soot formation and distribution. The formation of soot in industrial combustion systems is of interest in engineering, because the presence of soot in the flame enhances the heat transfer from the combustion gases by thermal radiation, increases the need for burner maintenance, and constitutes an environmental problem when emitted in the atmosphere.

International Communications in Heat and Mass Transfer 36[5], 445-450. 2009.

P098-09 "An instrument for combining x-ray multiple diffraction and x-ray topographic imaging for examining crystal microcrystallography and perfection"

Lai, X., Ma, C. Y., Roberts, K. J., Cardoso, L. P., dos Santos, A. O., Bogg, D., and Miller, M. C.

Diffraction imaging using x-ray topography (XRT) and x-ray multiple diffraction (XRMD) provide valuable tools for examining the growth defects in crystals and the distributions from ideal lattice symmetry (microcrystallography). The topographic x-ray multiple diffraction microprobe (TMDM) combines the complementary aspects of both techniques enabling XRT and XRMD studies within the same instrument providing a useful resource for the structural characterization of materials that are not very stable in vacuum and electron beam environments. The design of the TMDM instrument is described together with data taken on GaAs (001) and potassium dihydrogen phosphate (001)

Review of Scientific Instruments 80[3]. 033705. 2009.

P099-09 "Complete state reconstruction of a two-mode Gaussian state via local operations and classical communication"

Rigolin, G. and de Oliveira, M. C.

We propose a strictly local protocol that is completely equivalent to global quantum state reconstruction for a bipartite system. We show that the joint density matrix of an arbitrary two-mode Gaussian state, entangled or not, is obtained via local operations and classical communication only. In contrast to previous proposals, simultaneous homodyne measurements on both modes are replaced with local homodyne detections and a set of local projective measurements

Physical Review A 79[3]. 030302. 2009.

P100-09 "Characterization of lignocellulosic curaua fibres"

Spinace, M. A. S., Lambert, C. S., Fermoselli, K. K. G., and De Paoli, M. A.

Curaua fibres have specific mechanical properties similar to inorganic fibres and are an important renewable raw material. Milled curaua fibres, submitted to different treatments, were characterized by mechanical and thermal properties, moisture content, water absorption, surface morphology, FTIR spectroscopy, density and X-ray diffraction. Except for moisture content and mechanical properties, no other significant changes were observed after the treatments. The treated fibres also show an increase of surface roughness.

Carbohydrate Polymers 77[1]. 47-53. 2009.

P101-09 "Cross sections and asymmetry parameters for photoionization of CH3F in the VUV region"

dos Santos, A. S., Machado, L. E., Lee, M. T., Brescansin, L. M., and Lucchese, R. R.

Calculated cross sections and asymmetry parameters for photoionization of the three outermost valence orbitals of CH3F for photon energies from near threshold to 50 eV are reported. The photoelectron continuum orbitals are obtained using the Schwinger variational method at the level of static-exchange plus correlation potential. Our results are compared with other theoretical and experimental results showing a good quantitative agreement. Correlation effects do not significantly affect the computed total cross sections and photoelectron asymmetry parameters. The broader structure that appears in the experimental cross section are well described. However, the narrow resonant features near threshold are not found in the present one-electron treatment of the photoionization process.

Chemical Physics 358[1-2], 96-102. 2009.

P102-09 "Defects in Graphene-Based Twisted Nanoribbons: Structural, Electronic, and Optical Properties"

Caetano, E. W. S., Freire, V. N., dos Santos, S. G., Albuquerque, E. L., Galvao, D. S., and Sato, F.

We present some computational simulations of graphene-based nanoribbons with a number of half-twists varying from 0 to 4 and two types of defects obtained by removing a single carbon atom from two different sites. Optimized geometries are found by using a mix of classical quantum semiempirical computations. According with the simulations results, the local curvature of the nanoribbons increases at the defect sites, especially fora higher number of half-twists. The HOMO-LUMO energy gap of the nanostructures has significant variation when the number of half-twists increases for the defective nanoribbons. At the quantum semiempirical level, the first optically active transitions and oscillator strengths are calculated using the full configuration interaction (CI) framework, and the optical absorption in the UV/vis range (electronic transitions) and in the infrared (vibrational transitions) are achieved. Distinct nanoribbons show unique spectral signatures in the UV/vis range, with the first absorption peaks in wavelengths ranging from the orange to the violet. Strong absorption is observed in the ultraviolet region, although differences in their infrared spectra are hardly discernible

Langmuir 25[8], 4751-4759. 2009.

P103-09 "Diagnostic reference levels for the most frequent radiological examinations carried out in Brazil"

Freitas, M. B. and Yoshimura, E. M.

Objectives. A large-scale survey of doses to patients undergoing the most frequent radiological examinations was carried out in health services in Sao Paulo (347 radiological examinations per 1 000 inhabitants), the most populous Brazilian state. Methods. A postal dosimetric kit with thermoluminescence dosimeters was used to evaluate the entrance surface dose (ESD) to patients. A stratified sampling technique applied to the national health database furnished important data on the distribution of equipment and the annual number of examinations. Chest, head (skull and sinus), and spine (cervical, thoracic, and lumbar) examinations were included in the trial. A total of 83 rooms and 868 patients were included, and 1 415 values of ESD were measured. Results. The data show large coefficients of variation in tube charge, giving rise to large variations in ESD values. Also, a series of high ESD values associated with unnecessary localizing fluoroscopy were detected. Diagnostic reference levels were determined, based on the 75th percentile (third quartile) of the ESD distributions. For adult patients, the diagnostic reference levels achieved are very similar to those obtained in international surveys. However, the situation is different for pediatric patients: the ESD values found in this survey are twice as large as the international recommendations for chest radiographs of children. Conclusions. Despite the reduced number of ESD values and rooms for the pediatric patient group, it is recommended that practices in chest examinations be revised and that specific national reference doses and image quality be established after a broader survey is carried out

Revista Panamericana de Salud Publica-Pan American Journal of Public Health 25[2], 95-104. 2009.

P104-09 "Eeg-Fmri of Temporal Lobe Epilepsy: Source Localization Using Bold and Ica"

Sercheli, M., Bilevicius, E., Ozelo, H., Alessio, A., Pereira, F., Rondina, J., Cendes, F., and Covolan, R.

Epilepsia 50, 219-279. 2009.
In: Conference: 8th European Congress on Epileptology Location: Berlin, GERMANY Date: SEP 21-25, 2008.

P105-09 "EEG spike source localization before and after surgery for temporal lobe epilepsy: a BOLD EEG-fMRI and independent component analysis study"

Sercheli, M. S., Bilevicius, E., Alessio, A., Ozelo, H., Pereira, F. R. S., Rondina, J. M., Cendes, F., and Covolan, R. J. M.

Simultaneous measurements of EEG-functional magnetic resonance imaging (fMRI) combine the high temporal resolution of EEG with the distinctive spatial resolution of fMRI. The purpose of this EEG-fMRI study was to search for hemodynamic responses (blood oxygen level-dependent-BOLD responses) associated with interictal activity in a case of right mesial temporal lobe epilepsy before and after a successful selective amygdalohippocampectomy. Therefore, the study found the epileptogenic source by this noninvasive imaging technique and compared the results after removing the atrophied hippocampus. Additionally, the present study investigated the effectiveness of two different ways of localizing epileptiform spike sources, i.e., BOLD contrast and independent component analysis dipole model, by comparing their respective outcomes to the resected epileptogenic region. Our findings suggested a right hippocampus induction of the large interictal activity in the left hemisphere. Although almost a quarter of the dipoles were found near the right hippocampus region, dipole modeling resulted in a widespread distribution, making EEG analysis too weak to precisely determine by itself the source localization even by a sophisticated method of analysis such as independent component analysis. On the other hand, the combined EEG-fMRI technique made it possible to highlight the epileptogenic foci quite efficiently

Brazilian Journal of Medical and Biological Research 42[6], 582-587. 2009.

P106-09 "Electronic band effects on the spin disorder resistivity of Gd-4(Co1-xCux)(3) compounds"

Seixas, T. M., da Silva, M. A. S., de Lima, O. F., Lopez, J., Braun, H. F., and Eska, G.

We present a study of the spin disorder resistivity (rho(m infinity)) and the electronic specific heat coefficient (gamma) in Gd-4(Co1-xCux)(3) compounds, with x = 0.00, 0.05, 0.10, 0.20 and 0.30. The experimental results show a strongly nonlinear dependence of rho(m infinity) on the average de Gennes factor (G(av)) which, in similar intermetallic compounds, is usually attributed to the existence of spin fluctuations on the Co 3d bands.

Values of gamma were found around 110 mJ mol(-1) K-2 for the Gd-4(Co1-xCux)(3) compounds, much larger than 38.4 mJ mol(-1) K-2 found for the isostructural nonmagnetic Y4Co3 compound. Using a novel type of analysis we show that the ratio rho(m infinity)/ gamma(2) follows a well-defined linear dependence on G(av), which is expected when appropriate dependencies with the effective electron mass are taken into account. This indicates that band structure effects, rather than spin fluctuations, could be the main cause for the strong electron scattering and gamma enhancement observed in the Gd-4(Co1-xCux)(3) compounds. A discussion on relevant features of magnetization and electrical resistivity data, for the same series of compounds, is also presented

Journal of Physics-Condensed Matter 21[19]. 195603. 2009.

P107-09 "Energy and system size dependence of phi meson production in Cu plus Cu and Au plus Au collisions"

Abelev, B. I., Aggarwal, M. M., Ahammed, Z., Anderson, B. D., Arkhipkin, D., Averichev, G. S., Bai, Y., Balewski, J., Barannikova, O., Barnsby, L. S., et all

We study the beam-energy and system-size dependence of phi meson production (using the hadronic decay mode phi -> K+ K-) by comparing the new results from Cu + Cu collisions and previously reported Au + Au collisions at root s(NN) = 62.4 and 200 GeV measured in the STAR experiment at RHIC. Data presented in this Letter are from mid-rapidity (vertical bar y vertical bar < 0.5) for 0.4 < p(T) < 5 GeV/c. At a given beam energy, the transverse momentum distributions for phi mesons are observed to be similar in yield and shape for Cu + Cu and Au + Au colliding systems with similar average numbers of participating nucleons. The phi meson yields in nucleus-nucleus collisions, normalized by the average number of participating nucleons, are found to be enhanced relative to those from p + p collisions. The enhancement for phi mesons lies between strange hadrons having net strangeness = 1 (K- and <(A)over bar>) and net strangeness = 2 (Xi). The enhancement for phi mesons is observed to be higher at root s(NN) = 200 GeV compared to 62.4 GeV. These observations for the produced phi(s (s) over bar) mesons clearly suggest that, at these collision energies, the source of enhancement of strange hadrons is related to the formation of a dense partonic medium in high energy nucleus-nucleus collisions and cannot be alone due to canonical suppression of their production in smaller systems.

Physics Letters B 673[3], 183-191. 2009.

P108-09 "Engineering structural and magnetic properties of Mg0.95Mn0.05Fe2O4 thin films using 200 MeV Au ions"

Kumar, S., Sharma, S. K., Choudhary, R. J., Lee, C. G., Koo, B. H., Alimuddin, and Kumar, R.

Pulsed laser deposited thin films of Mg0.95Mn0.05Fe2O4 ferrite were irradiated by 200 MeV Au14+ with a maximum dose up to 1 x 10(12) ions/cm(2). The as-deposited and irradiated thin films are investigated using X-ray diffraction (XRD), Raman Spectroscopy, Field emission electron microscopy (FESEM) and de magnetization measurements. XRD and Raman spectroscopy measurements; reflect the cubic spinel structure of films before and after irradiation. FESEM measurements demonstrate that films are composed of nano rods and nanocrystalline grains. Magnetic hysteresis loop measurements reveal that all the films have ferrimagnetic ordering at room temperature with enhancement in the coercive field and remnant magnetization due to irradiation.

Journal of the Ceramic Society of Japan 117[1365], 685-688. 2009.

P109-09 "Enhanced side-mode suppression in chaotic stadium microcavity lasers"

Mestanza, S. N. M., Von Zuben, A. A., and Frateschi, N. C.

We report an enhanced side-mode suppression in Bunimovich stadium lasers with strained InGaAs/InGaP quantum well (QW) active regions. This is realized with spatially selective carrier injection along a particular periodic orbit of the stadium. The selectivity is achieved using He+3 ion implantation. Up to 21 dB enhancement in side-mode suppression is observed for a 40x20 mu m(2) stadium with interband transition between the first excited quantum well level. The improvement in side-mode suppression is apparently a consequence of coherent beating between orbits leading to a Vernier effect. A simple model corroborate with this hypothesis

Journal of Applied Physics 105[6]. 063101. 2009.

P110-09 "Inner and outer edge states in graphene rings: A numerical investigation"

Bahamon, D. A., Pereira, A. L. C., and Schulz, P. A.

We numerically investigate quantum rings in graphene and find that their electronic properties may be strongly influenced by the geometry, the edge symmetries, and the structure of the corners. Energy spectra are calculated for different geometries (triangular, hexagonal, and rhombus-shaped graphene rings) and edge terminations (zigzag, armchair, as well as the disordered edge of a round geometry). The states localized at the inner edges of the graphene rings describe different evolution as a function of magnetic field when compared to those localized at the outer edges. We show that these different evolutions are the reason for the formation of subbands of edge-states energy levels, separated by gaps (anticrossings). It is evident from mapping the charge densities that the anticrossings occur due to the coupling between inner and outer edge states

Physical Review B 79[12]. 125414. 2009.

P111-09 "Investigation of the first-order metamagnetic transitions and the colossal magnetocaloric effect using a Landau expansion applied to MnAs compound"

Carvalho, A. M. G., Coelho, A. A., Gama, S., Gandra, F. C. G., von Ranke, P. J., and de Oliveira, N. A.

We have explored a simple Landau model to calculate magnetization isotherms considering magnetic hysteresis. The model parameters have been chosen to fit the magnetic and magnetocaloric data of MnAs compound. Experimental data show that there is a great difference between the isothermal variation of the entropy (S-T) obtained from isotherms measured increasing and decreasing magnetic field. This great difference is reproduced theoretically. From the experimental and phenomenological isotherms, we calculated the S-T. From the theoretical entropy, we also obtained S-T, which does not present the colossal peak

European Physical Journal B 68[1], 67-72. 2009.

P112-09 "Landau levels in bulk graphite by Raman spectroscopy"

Garcia-Flores, A. F., Terashita, H., Granado, E., and Kopelevich, Y.

The electronic Raman scattering of bulk graphite at zero magnetic field reveals a structureless signal characteristic of a metal. For B greater than or similar to 2 T, several peaks at energies scaling linearly with magnetic field were observed and ascribed to transitions from the lowest energy Landau level(s) [LL(s)] to excited states belonging to the same ladder. The LLs are equally (unequally) spaced for high (low) quantum numbers, being consistent with the LL sequence from massive chiral fermions [m(*)=0.033(2)m(e)] with Berry's phase 2 pi found in graphene bilayers. These results provide spectroscopic evidence that some of the physics recently revealed by graphene multilayers is also shared by bulk graphite

Physical Review B 79[11]. 113105. 2009.

P113-09 "Laser-dressing effects on the electron g factor in low-dimensional semiconductor systems under applied magnetic fields"

Lopez, F. E., Reyes-Gomez, E., Brandi, H. S., Porras-Montenegro, N., and Oliveira, L. E.

The effects of a laser field on the conduction-electron effective Lande g factor in GaAs-Ga1-xAlxAs quantum wells and quantum-well wires under applied magnetic fields are studied within the effective-mass approximation. The interaction between the laser field and the semiconductor heterostructure is taken into account via a renormalization of the semiconductor energy gap and conduction-electron effective mass. Calculations are performed for the conduction-electron Lande factor and g-factor anisotropy by considering the non-parabolicity and anisotropy of the conduction band. Theoretical results are obtained as functions of the laser intensity, detuning and geometrical parameters of the low-dimensional semiconductor heterostructures, and indicate the possibility of manipulating and tuning the conduction-electron g factor in heterostructures by changing the detuning and laser-field intensity

Journal of Physics D-Applied Physics 42[11]. 115304. 2009.

P114-09 "Low-energy electron collisions with ethane"

Bettega, M. H. F., da Costa, R. F., and Lima, M. A. P.

We employed the Schwinger multichannel method to compute elastic cross sections for low-energy electron collisions with ethane (C2H6). The calculations were carried out in the static-exchange and static-exchange plus polarization approximations for energies up to 12 eV. Our integral cross section shows good agreement with experimental data and with theoretical results for energies above 5 eV. There are some differences for energies below 5 eV between our results and the available experimental and theoretical results. Our differential cross sections also agree well with the experiment and with theory for energies above 5 eV; below this energy our results agree in shape, but are smaller than the available experimental and theoretical results. We discuss possible reasons for these discrepancies. We found a broad structure in the integral cross section around 8.5 eV and also a Ramsauer-Townsend minimum around 0.2 eV. These results are in agreement with the experimental observations and theoretical results

Brazilian Journal of Physics 39[1], 69-73. 2009.

P115-09 "Martensitic transformation of Cu on Ag(001) and Cu on Au(001) studied with classical molecular dynamics"

Pereira, Z. S. and da Silva, E. Z.

The growth of Cu thin films on Ag(001) and Au(001) substrates was modeled using molecular dynamics with classical potentials. We observed that deposited atoms formed an unstable bcc or bcc/body-centered-tetragonal structure, in agreement with previous experiments. We show that the formation of such structures is related to film thickness and temperature that was analyzed in the interval from 200 to 600 K. bcc nucleation was measured by observing the relation between thickness and temperature of the deposited thin film. The martensitic transformation accompanied by a stripe pattern occurred as a consequence of the distortions caused by the underlying substrate lattice. The stripe patterns were measured as 57 and 61 A for Cu on Ag and Cu on Au, respectively. Monolayer spacing and coordination number of atoms were calculated, clearly evidencing the formed structures. Local structures were studied using the Ackland-Jones method, to determine the phases of the deposited films

Physical Review B 79[11]. 115404. 2009.

P116-09 "Magnetic characterization of Mn5SiB2 and Mn5Si3 phases"

de Almeida, D. M., Bormio-Nunes, C., Nunes, C. A., Coelho, A. A., and Coelho, G. C.

In this work the Mn5Si3 and Mn5SiB2 phases were produced via arc melting and heat treatment at 1000 degrees C for 50 h under argon. A detailed microstructure characterization indicated the formation of single-phase Mn5Si3 and near single-phase Mn5SiB2 microstructures. The magnetic behavior of the Mn5Si3 phase was investigated and the results are in agreement with previous data from the literature, which indicates the existence of two anti-ferromagnetic structures for temperatures below 98 K. The Mn5SiB2 phase shows a ferromagnetic behavior presenting a saturation magnetization M-s of about 5.35 x 10(5) A/m (0.67 T) at room temperature and an estimated Curie temperature between 470 and 490 K. In addition, AC susceptibility data indicates no evidence of any other magnetic ordering in 4-300 K temperature range. The magnetization values are smaller than that calculated using the magnetic moment from previous literature NMR results. This result suggests a probable ferrimagnetic arrangement of the Mn moments.

Journal of Magnetism and Magnetic Materials 321[17], 2578-2581. 2009.

P117-09 "Observation of Two-Source Interference in the Photoproduction Reaction AuAu -> AuAu rho(0)"

Abelev, B. I., Aggarwal, M. M., Ahammed, Z., Anderson, B. D., Arkhipkin, D., Averichev, G. S., Bai, Y., Balewski, J., Barannikova, O., et all

In ultraperipheral relativistic heavy-ion collisions, a photon from the electromagnetic field of one nucleus can fluctuate to a quark-antiquark pair and scatter from the other nucleus, emerging as a rho(0). The rho(0) production occurs in two well-separated (median impact parameters of 20 and 40 F for the cases considered here) nuclei, so the system forms a two-source interferometer. At low transverse momenta, the two amplitudes interfere destructively, suppressing rho(0) production. Since the rho(0) decays before the production amplitudes from the two sources can overlap, the two-pion system can only be described with an entangled nonlocal wave function, and is thus an example of the Einstein-Podolsky-Rosen paradox. We observe this suppression in 200 GeV per nucleon-pair gold-gold collisions. The interference is 87%+/- 5%(stat.)+/- 8%(syst.) of the expected level. This translates into a limit on decoherence due to wave function collapse or other factors of 23% at the 90% confidence level

Physical Review Letters 102[11]. 112301. 2009.

P118-09 "Speckle photo electromotive force in CdTe:V and CdTe:Ge for measurement of vibration with large amplitude"

dos Santos, T. O., Frejlich, J., Launay, J. C., and Shcherbin, K.

The photo-electromotive force induced by a speckle pattern vibrating with large amplitude in photorefractive CdTe:V and CdTe:Ge is experimentally studied. This technique is shown to be suitable for transversal amplitude vibration measurement as well as for material response time and associated conductivity characterization. Experiments were carried out with 532 and 1064 nm wavelength illumination over a wide vibration frequency range. The results are in good agreement with a previously reported theoretical model. The studied doped crystals exhibit peculiar different features that are described and discussed

Applied Physics B-Lasers and Optics 95[3], 627-632. 2009.

P119-09 "Structural and electrochemical characterization of a cobalt phthalocyanine bulk-modified SiO2/SnO2 carbon ceramic electrode"

Arguello, J., Magosso, H. A., Ramos, R. R., Canevari, T. C., Landers, R., Pimentel, V. L., and Gushikem, Y.

A cobalt phthalocyanine bulk-modified carbon ceramic composite has been prepared by using sol-gel processing, and characterized by BET surface area, X-ray photoelectron spectroscopy, scanning electron microscopy and atomic force microscopy. A water-soluble 3-n-propylpyridinium chloride silsesquioxane (SiPyCl), an ion exchanger polymer, was employed to attach cobalt(II) tetrasulfophthalocyanine (CoTsPc) and prevent its leakage, as well as, to ensure adequate dispersion in the sol-gel network. The modified electrode built in a rigid disk-format displayed good electrocatalytic behavior towards the oxidation of oxalic acid at 0.84V (SCE), as evidenced by the enhancement of the anodic current peak intensity when the concentration of oxalic acid was increased. A linear response was found in the range of 1.6 x 10(-5) to 1.5 x 10(-3) mol l(-1) with a detection limit of 7.1 x 10(-6) mol l(-1).

Electrochimica Acta 54[7], 1948-1953. 2009.

P120-09 "Systematic measurements of identified particle spectra in pp, d plus Au, and Au plus Au collisions at the STAR detector"

Abelev, B. I., Aggarwal, M. M., Ahammed, Z., Anderson, B. D., Arkhipkin, D., Averichev, G. S., Bai, Y., Balewski, J., Barannikova, O., et all

Identified charged-particle spectra of pi(+/-), K-+/-, p, and (p) over bar at midrapidity (vertical bar y vertical bar < 0.1) measured by the dE/dx method in the STAR (solenoidal tracker at the BNL Relativistic Heavy Ion Collider) time projection chamber are reported for pp and d + Au collisions at root s(NN) = 200 GeV and for Au + Au collisions at 62.4, 130, and 200 GeV. Average transverse momenta, total particle production, particle yield ratios, strangeness, and baryon production rates are investigated as a function of the collision system and centrality. The transverse momentum spectra are found to be flatter for heavy particles than for light particles in all collision systems; the effect is more prominent for more central collisions. The extracted average transverse momentum of each particle species follows a trend determined by the total charged-particle multiplicity density. The Bjorken energy density estimate is at least several GeV/fm(3) for a formation time less than 1 fm/c. A significantly larger net-baryon density and a stronger increase of the net-baryon density with centrality are found in Au + Au collisions at 62.4 GeV than at the two higher energies. Antibaryon production relative to total particle multiplicity is found to be constant over centrality, but increases with the collision energy. Strangeness production relative to total particle multiplicity is similar at the three measured RHIC energies. Relative strangeness production increases quickly with centrality in peripheral Au + Au collisions, to a value about 50% above the pp value, and remains rather constant in more central collisions. Bulk freeze-out properties are extracted from thermal equilibrium model and hydrodynamics-motivated blast-wave model fits to the data. Resonance decays are found to have little effect on the extracted kinetic freeze-out parameters because of the transverse momentum range of our measurements. The extracted chemical freeze-out temperature is constant, independent of collision system or centrality; its value is close to the predicted phase-transition temperature, suggesting that chemical freeze-out happens in the vicinity of hadronization and the chemical freeze-out temperature is universal despite the vastly different initial conditions in the collision systems. The extracted kinetic freeze-out temperature, while similar to the chemical freeze-out temperature in pp, d + Au, and peripheral Au + Au collisions, drops significantly with centrality in Au + Au collisions, whereas the extracted transverse radial flow velocity increases rapidly with centrality. There appears to be a prolonged period of particle elastic scatterings from chemical to kinetic freeze-out in central Au + Au collisions. The bulk properties extracted at chemical and kinetic freeze-out are observed to evolve smoothly over the measured energy range, collision systems, and collision centralities

Physical Review C 79[3]. 034909. 2009.

P121-09 "Test of chemical freeze-out at the RHIC"

Takahashi, J.

We present the results of a systematic test applying statistical thermal model fits in a consistent way for different particle ratios and different system sizes using the various particle yields measured in the STAR experiment. Comparison between central and peripheral Au+Au and Cu+Cu collisions with data from p+p collisions provides an interesting tool to verify the dependence on the system size. We also present a study of the rapidity dependence of the thermal fit parameters using available data from the RHIC in the forward rapidity regions and also using different parameterizations for the rapidity distribution of different particles

Journal of Physics G-Nuclear and Particle Physics 36[6]. 064074. 2009.

P122-09 "Thermal Behavior, Microstructure, Polymorphism, and Crystallization Properties of Zero Trans Fats from Soybean Oil and Fully Hydrogenated Soybean Oil"

Ribeiro, A. P. B., Grimaldi, R., Gioielli, L. A., dos Santos, A. O., Cardoso, L. P., and Goncalves, L. A. G.

Blends of soybean oil (SO) and fully hydrogenated soybean oil (FHSBO), with 10, 20, 30, 40, and 50% (w/w) FHSBO content were interesterified under the following conditions: 20 min reaction time, 0.4% sodium methoxide catalyst, and 500 rpm stirring speed, at 100 A degrees C. The original and interesterified blends were examined for triacylglycerol composition, thermal behavior, microstructure, crystallization kinetics, and polymorphism. Interesterification produced substantial rearrangement of the triacylglycerol species in all the blends, reduction of trisaturated triacylglycerol content and increase in monounsaturated-disaturated and diunsaturated-monosaturated triacylglycerols. Evaluation of thermal behavior parameters showed linear relations with FHSBO content in the original blends. Blend melting and crystallization thermograms were significantly modified by the randomization. Interesterification caused significant reductions in maximum crystal diameter in all blends, in addition to modifying crystal morphology. Characterization of crystallization kinetics revealed that crystal formation induction period (tau (SFC)) and maximum solid fat content (SFCmax) were altered according to FHSBO content in the original blends and as a result of the random rearrangement. Changes in Avrami constant (k) and exponent (n) indicated, respectively, that-as compared with the original blends-interesterification decreased crystallization velocities and modified crystallization processes, altering crystalline morphology and nucleation mechanism. X-ray diffraction analyses revealed that interesterification altered crystalline polymorphism. The interesterified blends showed a predominance of the beta' polymorph, which is of more interest for food applications

Food Biophysics 4[2], 106-118. 2009.

P123-09"Vanadium-doped photorefractive titanosillenite crystal"

Montenegro, R., Shumelyuk, A., Kumamoto, R., Carvalho, J. F., Santana, R. C., and Frejlich, J.

Holographic recording in a vanadium-doped B12TiO20 (BTO) photorefractive crystal puts into evidence a large hole-electron competition showing a fast and a slow hologram components. From the fast component evolution, some material parameters for the electron-donor photoactive centers are computed.

The wavelength-resolved photoconductivity is shown to be strongly modified by V-doping compared to undoped and doped BTO with other elements. The increase of photoconductivity by green light preexposure is almost negligible here if compared with undoped BTO. Activation energy for dark conductivity measured for BTO:V is similar to that for undoped BTO, as measured close to room temperature, but sensibly lower than the value reported in the literature for a much higher temperature range. Optical absorption and EPR spectra do confirm already published results and suggestions about the possible role of vanadium in the sillenite structure.

Applied Physics B-Lasers and Optics 95[3], 475-482. 2009.

Abstracta

Instituto de Física
Diretor: Prof. Dr. Julio Cesar Hadler Neto
Universidade Estadual de Campinas - UNICAMP
Cidade Universitária Zeferino Vaz
13083-859 - Campinas - SP - Brasil
e-mail: secdir@ifi.unicamp.br
Fone: 0XX 19 3521-5300

Publicação

Biblioteca do Instituto de Física Gleb Wataghin
http://webbif.ifi.unicamp.br
Diretora Técnica: Sandra Maria Carlos Cartaxo

Elaboração
Antonela Carvalho Ribeiro
antonela@ifi.unicamp.br

Projeto Gráfico
ÍgneaDesign

Impressão

Gráfica Central - Unicamp